Available online at www.sciencedirect.com
ScienceDirect
Journal of Power Sources 161 (2006) 444–453
JOURNAL OF POWER SOURCES
www.elsevier.com/locate/jpowsour

Effects of the electrical resistances of the GDL in a PEM fuel cell

Tianhong Zhou, Hongtan Liu *

Department of Mechanical Engineering, University of Miami, Coral Gables, FL 33124, USA

Received 2 March 2006; received in revised form 18 April 2006; accepted 19 April 2006
Available online 9 June 2006

Abstract

In most PEM fuel cell models, the electrical resistance of the gas diffusion layers (GDL) is neglected under the assumptions that the GDL electrical conductivity is orders of magnitude higher than the ionic conductivity of the membrane. Recently some modeling efforts have taken the effects of electrical resistance of the GDL into consideration [H. Meng, C.Y. Wang, Electron transport in PEFCs, J. Electrochem. Soc. 151 (2004) A358–A367; B.R. Sivertsen, N. Djilali, CFD-based modeling of proton exchange membrane fuel cells, J. Power Sources 141 (2005) 65–78] and some of the results showed that under certain conditions, this effect was significant enough to alter the characteristics of current density distributions under the gas channels and the land areas. If these results are applicable to real-life fuel cells, the present design criteria and optimization procedures must be significantly changed to incorporate the effect of GDL electrical resistance. To examine this issue closely, a three-dimensional fuel cell model incorporating electron transport in the GDL is developed and employed to investigate the effect of electrical resistance through the GDL. In this model, the anisotropic nature of the GDL is taken into consideration by using different electrical conductivities in the through-plane and in-plane directions. The modeling results show that when realistic electrical conductivities for the GDL are used, the effect of the electrical resistance of GDL is slight and can be neglected for all industrial applications. It is believed that the over-estimations of the GDL resistance were mainly caused by neglecting the anisotropic nature of the GDL and/or lumping the contact resistance indiscriminately into the GDL, thus overestimating the electrical resistance of the GDL in the in-plane direction. Besides taking into consideration of the electrical resistance of GDL, the present model also take into consideration of the electron transport in the catalyst layers. When realistic values of electrical conductivities are used for both the GDL and catalyst layers, there is no significant change in the characteristics of current density distribution across the land and channel.

Keywords: Fuel cell; Model; GDL electrical resistance

1. Introduction

During recent years, tremendous amount of efforts have been concentrated on modeling of proton exchange membrane fuel cells. In most of the modeling work, the transportation of protons inside the membrane and the ohmic losses by the proton current were included, while the electronic resistance of GDL and catalyst layer (CL), as well as the electrical losses by the electron current were omitted. The electron transport in the GDL and catalyst layer was neglected by assuming a sufficiently large electrical conductivity and, consequently, a uniform electronic phase potential in these materials. In recent years, some concerns over the electrical resistances of GDL have been raised [1,2].

The principle of the electrochemical reaction within the PEM fuel cell can be shown in Fig. 1. In the anode catalyst layer, hydrogen is consumed to produce protons and electrons. Electrons pass through an external circuit to the cathode, thus providing electrical power, while the protons transport through the membrane to the cathode. In the cathode catalyst layer, oxygen combines with protons and electrons to produce water. The transport paths of protons and electrons form a closed electrical circuit as shown in Fig. 1.

The electrical resistance in the GDL can cause a non-uniform distribution of the phase potential in the GDL, and thus causes an uneven distribution of overpotential. The local current density distribution is the result of the combined effects of non-uniform distributions of overpotential and reactant concentration. From the Butler–Volmer equation it is clear that the current generation rate in the cathode is linearly proportional to oxygen concentration, but increases exponentially with overpotential. Thus, a slight change in overpotential may have a significant effect

* Corresponding author. Tel.: +1 3052 842 019; fax: +1 3052842580.
E-mail address: hliu@miami.edu (H. Liu).

0378-7753/$ – see front matter © 2006 Elsevier B.V. All rights reserved.
doi:10.1016/j.jpowsour.2006.04.106

Nomenclature

$(ai_o^{ref})_a$	reference exchange current density times area at anode (A m^{-3})
$(ai_o^{ref})_c$	reference exchange current density times area at cathode (A m^{-3})
c	mole concentration (mol m^{-3})
$c_{O_2,ref}$	reference mole concentration of oxygen
$c_{H_2,ref}$	reference mole concentration of hydrogen
c_p	specific heat at constant pressure (J kg^{-1} K^{-1})
D	diffusivity (m^2 s^{-1}, cm^2 s^{-1})
E	fuel cell voltage (V)
E_0	open circuit potential (V)
F	Faraday constant (96487 C mol^{-1})
i_0	exchange current density (A m^{-2})
I, i	current density (A m^{-2})
j	transfer current density (A m^{-3})
k	thermal conductivity (W m^{-1} K^{-1})
k_φ	electrokinetic permeability (m^{-2})
k_p	hydraulic permeability of the porous medium (m^{-2})
L	thickness (m)
P	pressure, partial pressure (Pa)
$r^{(2)}$	coefficient in the generalized Darcy's equation
R	universal gas constant (8314 J mol^{-1} K^{-1})
S	source term of the species transport equation
T	temperature (K)
$\mathbf{V}$	velocity vector (m s^{-1})
x	dimension along gas flow direction
X	mole fraction
y	dimension along the direction from cathode to anode
z	dimension along the direction across the gas channel and shoulder

Greek symbols

α_a	anodic transfer coefficient
α_c	cathodic transfer coefficient
ε	porosity, volume fraction
ϕ	potential (V)
η	electrode overpotential (V)
μ	viscosity (kg m^{-1} s^{-1})
ρ	density (kg m^{-3})
σ	ionic conductivity, electronic conductivity (S m^{-1})

Subscripst and Superscripts

a	anode, anodic
c	cathode, cathodic
cl	catalyst layer
e	electron
eff	effective, accounting for porous medium
k	k'th component
m	membrane
p	proton
pore	porous media
ref	reference
s	solid

on current density. Recently, some researchers [1,2] took into consideration of the electronic resistance of the GDL in their modeling efforts and concluded that under certain fuel cell operating conditions, the maximum local current density may not be over the gas channel as previous results have shown [3,4]. However, in these studies the anisotropic nature of GDL conductivity was not taken into consideration, thus the results may not be applicable to real-life fuel cell situations. Sun et al. [5] presented a 2D cross-the channel model to investigate the influence of GDL property and flow-field geometry on the reaction distribution in the cathode catalyst layer. In one of cases studied, a 10-fold higher conductivity in the in-plane direction was used and the result showed that higher current density occurs under the land when compression of the GDL was not taken into consideration. Thus all three papers showed that the effect of electrical resistance of the GDL is significant enough to alter the characteristics of the current distribution and cause the current density to be higher under the land than that over the channel.

Commonly used gas diffusion layers are made of either carbon cloth or carbon fiber paper, both of which are highly anisotropic. Williams et al. [6] measured the in-plane conductivities of eight commercial gas diffusion layers and found that the electrical conductivity in the in-plane direction is between 0.48 and 2.33×10^4 S m^{-1}. The GDLs provided by Toray Industries Inc. have through-plane electrical conductivity about 1250 S m^{-1} (http://fuelcellstore.com/products/toray/specs.pdf), and the in-plane electrical conductivity about 1.72–2.13 $\times$ 10^4 S m^{-1}. The in-plane electrical conductivities are about 14–17 times of that in the through-plane direction. More information regarding the GDL characterization can be found in Barbir [7], where properties of typical fuel cell gas diffusion layers are summarized and the listed electrical conductivity

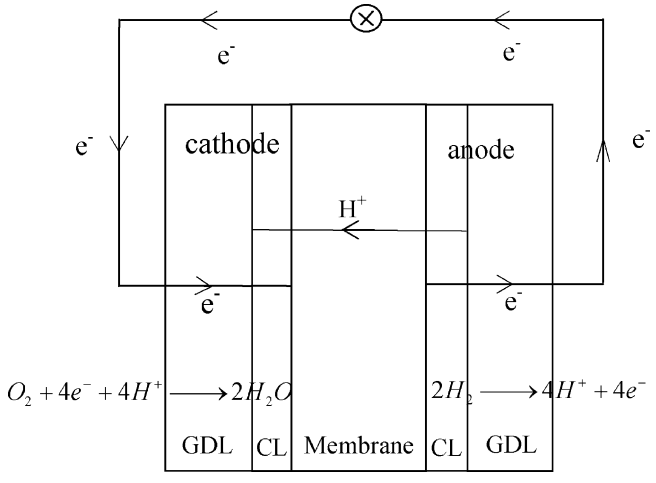

Fig. 1. Transporting paths of protons and electrons within PEMFC.

ranges from 14 to 1250 S m^{-1}. Note also that the contact resistance causes a resistance increase in the through-plane direction and has a minimal effect on the in-plane direction.

In this paper, the anisotropic properties of the GDL conductivity is taken into consideration directly in the modeling practice and realistic values for both in-plane and through-plane directions were used to study the effect of electrical resistance of the GDL. Additionally, electronic transport equation is also solved in the catalyst layer.

2. Computational model

The computation model is an extension from our previous fuel cell models [3,4], where detailed model description and model assumptions of the full 3D model can be found. The model geometry is a single PEM fuel cell as shown in Fig. 2.

The main governing equations include:

Continuity equation:

$$\nabla \cdot \rho \mathbf{V} = 0 \tag{1}$$

Momentum equation:

$$\rho \mathbf{V} \cdot (\nabla \mathbf{V}) = -\nabla \mathbf{P} + \begin{cases} \mu \Delta \mathbf{V} & \text{gas chanel} \\ r^{(2)} \mu \Delta \mathbf{V} - \varepsilon \dfrac{\mu}{k_\mathrm{p}} \mathbf{V} & \text{gas diffuser} \\ r^{(2)} \mu \Delta \mathbf{V} - \varepsilon \dfrac{\mu}{k_\mathrm{p}} \mathbf{V} + \varepsilon C_{\mathrm{H}^+} F k_\phi \dfrac{\nabla \phi}{k_\mathrm{p}} & \text{catalyst layer and membrane} \end{cases} \tag{2}$$

Energy equation:

$$\rho c_\mathrm{p} \mathbf{V} \cdot (\nabla T) = \varepsilon k_\mathrm{eff} \nabla^2 T + \begin{cases} 0 & \text{gas channel} \\ S_\mathrm{T} & \text{catalyst layer, membrane and GDL} \end{cases} \tag{3}$$

Species equation:

$$\rho \mathbf{V} \cdot (\nabla X_k) = \varepsilon \rho D_\mathrm{eff} \Delta X_k + \begin{cases} 0 & \text{gas channel and gas diffuser} \\ \varepsilon \rho S_k & \text{catalyst layer} \end{cases} \tag{4}$$

where k denotes the species. At the cathode, the mass generation source terms for oxygen, water and protons are $j_\mathrm{c}/(4Fc)$, $-j_\mathrm{c}/(2Fc)$, and $j_\mathrm{c}/(Fc)$, respectively. At the anode, the source terms for hydrogen and protons are $-j_\mathrm{a}/(2Fc)$, and j_a/Fc, respectively. j_a and j_c are the reaction rates, calculated from Butler–Volmer expression [8],

$$j_\mathrm{a} = (a i_0^{\mathrm{ref}})_\mathrm{a} \left(\frac{X_{H_2}}{X_{H_{2\mathrm{ref}}}} \right)^{\frac{1}{2}} \left[\exp\left(\frac{\alpha_\mathrm{a}^\mathrm{a} F}{RT} \eta_\mathrm{a} \right) - \exp\left(-\frac{\alpha_\mathrm{c}^\mathrm{a} F}{RT} \eta_\mathrm{a} \right) \right] \tag{5}$$

$$j_\mathrm{c} = (a i_0^{\mathrm{ref}})_\mathrm{c} \left(\frac{X_{\mathrm{O}_2}}{X_{\mathrm{O}_{2\mathrm{ref}}}} \right) \left[\exp\left(\frac{\alpha_\mathrm{a}^\mathrm{c} F}{RT} \eta_\mathrm{c} \right) - \exp\left(-\frac{\alpha_\mathrm{c}^\mathrm{c} F}{RT} \eta_\mathrm{c} \right) \right] \tag{6}$$

At the anode, the transfer coefficients in Eq. (5) are $\alpha_\mathrm{a}^\mathrm{a} = \alpha_\mathrm{c}^\mathrm{a} = 0.5$ [9,10]. At the cathode, $\alpha_\mathrm{c}^\mathrm{c} = 1$ and $\alpha_\mathrm{a}^\mathrm{c} = 0$ are used. At low overpotential, $a \approx 1$ and at high overpotential, $a \approx 0.6$–0.7 [11]. Since at high overpotential, the first term in the bracket of Eq. (6) is very small compared to the second term and thus can be neglected in the calculation. So in this work, $\alpha_\mathrm{c}^\mathrm{c} = 1$ and $\alpha_\mathrm{a}^\mathrm{c} = 0$ are used throughout of the overpotential range.

The overpotential within the catalyst layer is:

$$\eta = \phi_\mathrm{s} - \phi_\mathrm{p} - E_0 \quad \text{at cathode} \tag{7}$$

$$\eta = \phi_\mathrm{s} - \phi_\mathrm{p} \quad \text{at anode} \tag{8}$$

where E_0 is the open circuit voltage, φ_s is the solid phase potential and φ_p is the membrane phase potential.

The heat source term S_T includes both the heat generated from the overpotential and the ohmic heating of both proton and electron currents,

$$S_\mathrm{T} = \begin{cases} \eta \cdot j + \dfrac{i_\mathrm{p}^2}{\sigma_\mathrm{ct}^\mathrm{p}} + \dfrac{i_\mathrm{e}^2}{\sigma_\mathrm{ct}^\mathrm{e}} & \text{catalyst layer} \\ \dfrac{\mathrm{i}_\mathrm{p}^2}{\sigma_\mathrm{m}} & \text{membrane} \\ \dfrac{\mathrm{i}_\mathrm{e}^2}{\sigma_\mathrm{GDL}^\mathrm{e}} & \text{GDL} \end{cases} \tag{9}$$

The proton current satisfies:

$$\nabla \cdot i_\mathrm{p} = \begin{cases} j_\mathrm{c} & \text{cathode catalyst layer} \\ 0 & \text{membrane} \\ j_\mathrm{a} & \text{anode catalyst layer} \end{cases} \tag{10}$$

The electron current satisfies:

$$\nabla \cdot i_\mathrm{e} = \begin{cases} -j_\mathrm{c} & \text{cathode catalyst layer} \\ 0 & \text{GDL and shoulder} \\ -j_\mathrm{a} & \text{anode catalyst layer} \end{cases} \tag{11}$$

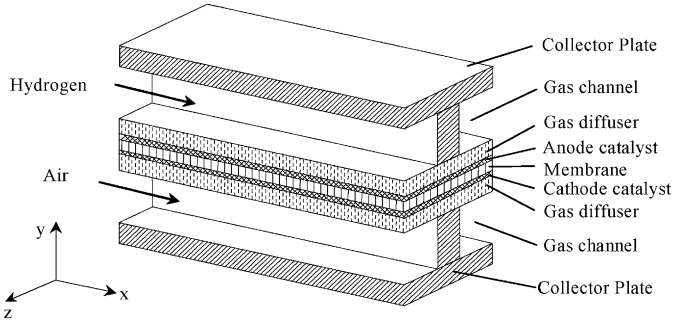

Fig. 2. A single PEM fuel cell [3].

From Eqs. (11) and (12), proton and electron current densities satisfy:

$$\nabla i_{\mathrm{p}} + \nabla i_{\mathrm{e}} = 0 \tag{12}$$

or

$$i_{\mathrm{p}} + i_{\mathrm{e}} = \text{constant} \tag{13}$$

Since the proton current is related to the membrane-phase potential by:

$$\begin{aligned} i_{\mathrm{p},x} &= -\sigma_{\mathrm{p},x}\frac{\partial \phi_{\mathrm{p}}}{\partial x} \\ i_{\mathrm{p},y} &= -\sigma_{\mathrm{p},y}\frac{\partial \phi_{\mathrm{p}}}{\partial y} \\ i_{\mathrm{p},z} &= -\sigma_{\mathrm{p},z}\frac{\partial \phi_{\mathrm{p}}}{\partial z} \end{aligned} \tag{14}$$

thus the membrane-phase potential satisfies:

$$\begin{aligned} &\frac{\partial}{\partial x}\left(\sigma_{\mathrm{p},x}\frac{\partial \phi_{\mathrm{p}}}{\partial x}\right) + \frac{\partial}{\partial y}\left(\sigma_{\mathrm{p},y}\frac{\partial \phi_{\mathrm{p}}}{\partial y}\right) + \frac{\partial}{\partial z}\left(\sigma_{\mathrm{p},z}\frac{\partial \phi_{\mathrm{p}}}{\partial z}\right) = j_{\mathrm{c}} \quad \text{cathode catalyst layer} \\ &\frac{\partial}{\partial x}\left(\sigma_{\mathrm{p},x}\frac{\partial \phi_{\mathrm{p}}}{\partial x}\right) + \frac{\partial}{\partial y}\left(\sigma_{\mathrm{p},y}\frac{\partial \phi_{\mathrm{p}}}{\partial y}\right) + \frac{\partial}{\partial z}\left(\sigma_{\mathrm{p},z}\frac{\partial \phi_{\mathrm{p}}}{\partial z}\right) = 0 \quad \text{membrane} \\ &\frac{\partial}{\partial x}\left(\sigma_{\mathrm{p},x}\frac{\partial \phi_{\mathrm{p}}}{\partial x}\right) + \frac{\partial}{\partial y}\left(\sigma_{\mathrm{p},y}\frac{\partial \phi_{\mathrm{p}}}{\partial y}\right) + \frac{\partial}{\partial z}\left(\sigma_{\mathrm{p},z}\frac{\partial \phi_{\mathrm{p}}}{\partial z}\right) = j_{\mathrm{a}} \quad \text{anode catalyst layer} \end{aligned} \tag{15}$$

Similarly, the solid-phase potential satisfies:

$$\begin{aligned} &\sigma_{\mathrm{e},x}\frac{\partial^2 \phi_{\mathrm{s}}}{\partial x^2} + \sigma_{\mathrm{e},y}\frac{\partial^2 \phi_{\mathrm{s}}}{\partial y^2} + \sigma_{\mathrm{e},z}\frac{\partial^2 \phi_{\mathrm{s}}}{\partial z^2} = -j_{\mathrm{c}} \quad \text{cathode catalyst layer} \\ &\sigma_{\mathrm{e},x}\frac{\partial^2 \phi_{\mathrm{s}}}{\partial x^2} + \sigma_{\mathrm{e},y}\frac{\partial^2 \phi_{\mathrm{s}}}{\partial y^2} + \sigma_{\mathrm{e},z}\frac{\partial^2 \phi_{\mathrm{s}}}{\partial z^2} = 0 \quad \text{GDL and shoulder} \\ &\sigma_{\mathrm{e},x}\frac{\partial^2 \phi_{\mathrm{s}}}{\partial x^2} + \sigma_{\mathrm{e},y}\frac{\partial^2 \phi_{\mathrm{s}}}{\partial y^2} + \sigma_{\mathrm{e},z}\frac{\partial^2 \phi_{\mathrm{s}}}{\partial z^2} = -j_{\mathrm{a}} \quad \text{anode catalyst layer} \end{aligned} \tag{16}$$

Note that the electrical conductivities of the solid in each direction are taken as constant.

Most of the boundary conditions are the same as in [4,5]. Additional boundary conditions are the ones for the solid-phase potential and electron current. As electrons cannot conduct through the membrane, the electron current density at the interface between the catalyst layer and the membrane is set to zero. Similarly, as protons cannot conduct through the GDL, the proton current density at the interface between the catalyst layer and the GDL is zero, too. Following the definition that the potential of a standard hydrogen electrode is zero, the value of potential along the anode collector plate edge is assumed 0, thus along the cathode collector plate edge, the potential is the cell voltage E.

The computation starts with the independent variable of cell voltage E. From the computational iterations, the corresponding current density, as well as the values of cathode and anode overpotential are determined, then the polarization curve is obtained.

3. Results and discussion

The geometric parameters and operation conditions used in the modeling practice are listed in Table 1. Different GDL electrical conductivities are used for the in-plane and through-plane directions. The electrical conductivities given by Toray's Industries Inc. were used as the base case values. In the through-plane direction, the electrical conductivity is taken to be $1250\ \mathrm{S\,m^{-1}}$, while in the in-plane direction, the electrical conductivity is taken to be $17200\ \mathrm{S\,m^{-1}}$. Cases with much lower GDL conductivities are also studied.

The catalyst layer usually consists of nanoscale platinum particles supported by microscale carbon particles, which are loosely embedded in a matrix of ionomer. Thus catalyst layer is usually very porous and isotropic macroscopically. In a catalyst layer carbon and platinum particles are electrically conductive. Thus the effective electrical conductivity of the solid volume can be estimated as:

$$\sigma_{\mathrm{s}}^{\mathrm{e}} = \sigma_{\mathrm{c}}^{\mathrm{e}}\varepsilon_{\mathrm{carbon}} + \sigma_{\mathrm{p}}^{\mathrm{e}}\varepsilon_{\mathrm{platinum}} \tag{17}$$

where $\varepsilon_{\mathrm{carbon}}$ and $\varepsilon_{\mathrm{platinum}}$ are the volumetric fractions of carbon and platinum in the catalyst layer solid volume, $\sigma_{\mathrm{c}}^{\mathrm{e}}$ and $\sigma_{\mathrm{p}}^{\mathrm{e}}$ are the electrical conductivities of carbon and platinum, respectively. As the volume fraction of platinum is very small and the platinum particles are highly dispersed and not a continuum, the electrical conductivity of the solid mass mainly depends on the volume fraction of carbon and its electrical conductivity. To calculate the effective electrical conductivity of the porous catalyst layer, an equation similar to the one used by Dagan [12] to estimate the effective heat conductivity can be used:

$$\sigma_{\mathrm{eff}}^{\mathrm{e}} = -2\sigma_{\mathrm{s}}^{\mathrm{e}} + \frac{1}{(\varepsilon/(2\sigma_{\mathrm{s}}^{\mathrm{e}} + \sigma_{\mathrm{pore}})) + ((1-\varepsilon)/3\sigma_{\mathrm{s}}^{\mathrm{e}})} \tag{18}$$

where σ_{pore} is the electrical conductivity of pores (both gas and liquid filled). Omitting the electrical conductivity of the pores, Eq. (2) can be simplified to:

$$\sigma_{\mathrm{eff}}^{\mathrm{e}} = \sigma_{\mathrm{s}}^{\mathrm{e}} \times \frac{2-2\varepsilon}{\varepsilon+2} \tag{19}$$

Pantea et al. [13] measured electrical conductivities of 10 different kinds of carbon blacks. With 30% carbon composition, the Black Pearl™ carbon black has an electrical conductivity of about $220\ \mathrm{S\,m^{-1}}$. Assuming carbon comprises 40% of the solid

Table 1
Base-case electrode parameters and properties

Gas channel length, 8.0×10^{-1} m
Gas channel height, 8.0×10^{-4} m
Gas diffuser height, 2.0×10^{-4} m
Catalyst layer height, 0.1×10^{-4} m
Gas channel width, 8×10^{-4} m
Collector width, 8×10^{-4} m
Membrane height, 0.3×10^{-4} m
Gas diffuser porosity, $\varepsilon = 0.6$
Catalyst layer porosity, $\varepsilon = 0.6$
Volume fraction membrane in catalyst layer, $\varepsilon_{mc} = 0.4$
Permeability to air of the gas diffuser, $k_p = 1.76 \times 10^{-11}$ m^2
Hydraulic permeability of membrane, $k_m = 1.58 \times 10^{-18}$ m^2
Ionic conductivity of the membrane, $\sigma_m = 10\,\Omega^{-1}$ m^{-1}
Reference exchange current density times area at cathode, $a\ j_0^{ref} = 1.69 \times 10^5$ A m^{-3}
Reference exchange current density times area at anode, $a\ jc_0^{ref} = 5 \times 10^8$ A m^{-3}
Oxygen reference concentration = 3.39 mol m^{-3}
Hydrogen reference concentration = 56.4 mol m^{-3}
Air inlet pressure, $p_i = 1$ atm
Cathode flow rate, $U_i = 1800$ sccm
Air inlet temperature = 70 °C
Oxygen/nitrogen ratio in air at inlet, 0.21/0.79
Hydrogen inlet pressure, $p_i = 1$ atm
Anode flow rate = 1000 sccm
Hydrogen inlet temperature = 70 °C
Electrical conductive of shoulder = 20,000 S m^{-1}
At anode, transfer coefficients in Eq. (5): $\alpha_a^a = \alpha_c^a = 0.5$
At cathode, transfer coefficients in Eq. (6): $\alpha_c^c = 1$, $\alpha_a^c = 0$

mass, then from Eq. (17), the electrical conductivity of the catalyst layer solid mass may have an electrical conductivity about 290 S m^{-1}. Further considering that the porosity of the catalyst layer is 0.6, the effective electrical conductivity calculated from Eq. (19) is about 90 S m^{-1}.

In an attempt to study the effects of electrical resistance of the catalyst layer and GDL, much lower values of electrical conductivity are also used in the computations. The cases studied are summarized in Table 2. In addition, a reference case with the electrical resistances of the GDL and catalyst layers neglected is also included.

Fig. 3 shows an example of the distribution of solid-phase potential ϕ_s and electron flows within catalyst layer, GDL and collector plate shoulder across the oyz plane. At the anode (Fig. 3(a)), electrons generated within the catalyst layer pass through GDL, and exits through the collector plate shoulder. At the cathode (Fig. 3(b)), electrons enter the cathode via the collector plate shoulder, and are consumed within the catalyst layer by the electro-chemical reaction. Fig. 4 shows the distribution of membrane-phase potential ϕ_p and proton transport within the membrane electrode assembly. Protons generated within the anode catalyst layer pass through the membrane and are consumed inside the cathode catalyst layer. The flow of protons shown in Fig. 4, along with the flow of electrons shown in Fig. 3, forms a close electrical circuit.

In Fig. 3(a), the electrons in the region under the channel have to flow to the region under the shoulder before exiting through the collector plate shoulder as the gas channel is not electrically conductive. Similarly, at the cathode (Fig. 3(b)), the electrons have to flow through the shoulder and transport from the region over the shoulder to the region over the gas channel. This causes a gradient in the solid phase potential. At the cathode, the value of $\phi_s - E_0$ is lower over the shoulder as shown in Fig. 5, where the variations of phase potentials across the z-direction are shown. In contrast to the distribution of the solid-phase potential, the membrane-phase potential ϕ_p is higher over the shoulder. From Eq. (7), cathode overpotential equals the difference between the ϕ_p and $\phi_p - E_0$, so the absolute value of the overpotential is lower over the channel than over the shoulder. It is the magnitude of j or η that better represents the chemical reaction rates, as shown in Eq. (6). Thus in Fig. 6(a) the absolute value of η is plotted. The distribution of $|\eta|$ in Fig. 6(a) is directly opposite to the distribution of oxygen shown in Fig. 6(b). Because the major mass transfer mechanism is mass diffusion in the GDL, oxygen concentration is naturally higher in the region directly over the gas channel than that in the region over the shoulder. From Eq. (5), the magnitude of chemical reaction depends on the combined effects of overpotential and oxygen concentration. This may lead to situations that the maximum current density is not directly over the channel, but such a situation mandates a much higher electrical resistance than the true values in a practical GDL.

Fig. 7a shows the distribution of overpotential (absolute values) inside cathode catalyst layer. The choice of absolute values is such that in Eq. (5) the absolute values indicate the magnitude of the current, and the signs indicate whether it is current generation or consumption. Across the z-direction, over the shoulder

Table 2
Computation cases

Cases	GDL electrical conductivity in-plane (x, z)	GDL electrical conductivity through plane (y)	Catalyst layer electrical conductivity	Power reduction when compared with Case 5	Power reduction when compared with Case 2
Case 1 (base case)	17200 S m^{-1} [a]	1250 S m^{-1} [a]	90 S m^{-1} [b]	0.63%	–
Case 2	1500 S m^{-1}	300 S m^{-1}	90 S m^{-1}	1.69%	–
Case 3	300 S m^{-1}	300 S m^{-1}	90 S m^{-1}	3.0%	1.3%
Case 4	100 S m^{-1}	300 S m^{-1}	90 S m^{-1}	5.3%	3.7%
Case 5	Not considering electrical losses			–	–
Case 6	GDL thickness doubled			3.55%	–
Case 7	GDL thickness reduced by 10 times			3.42%	–

[a] Data from Toray Industries Inc.(fuelcellstore.com/products/toray/specs.pdf).
[b] Data computed from the electrical conductivity of carbon blacks and catalyst layer porosity.

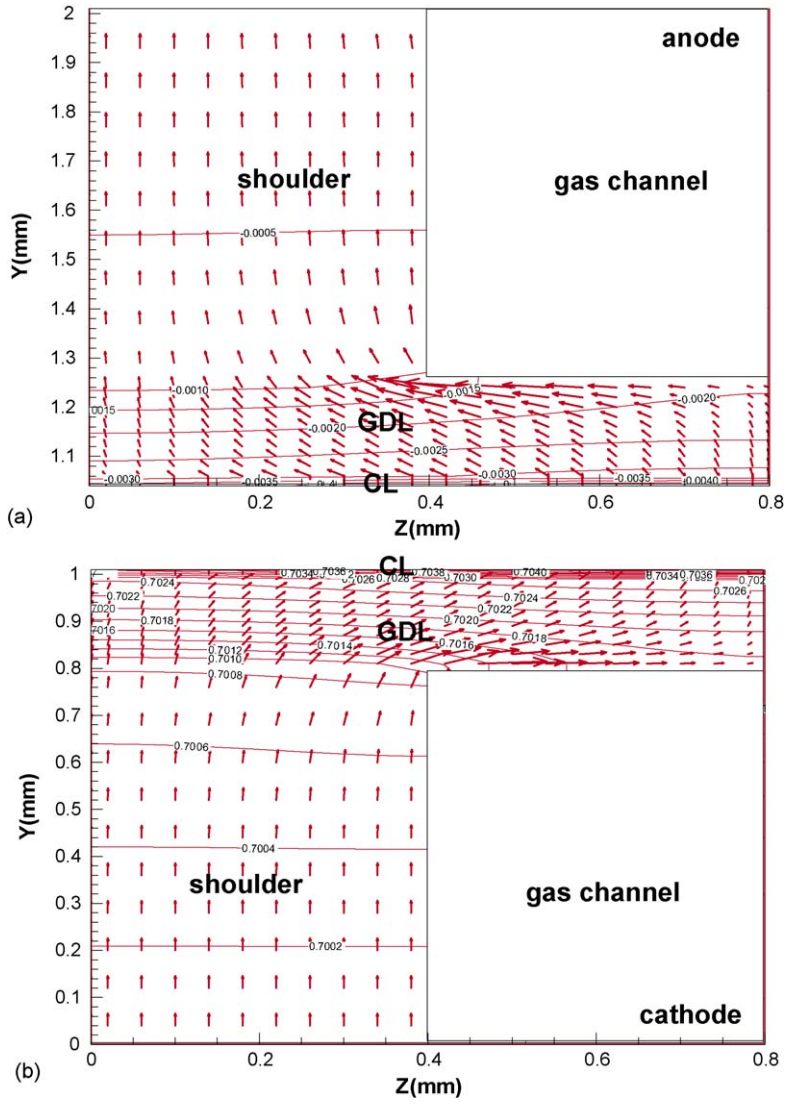

Fig. 3. Solid-phase potential and electron transportation within the fuel cell (a) at anode (b) at cathode, $x = 0.2$ m. Current density = 0.7817 A cm^{-2}, cell voltage = 0.7 V.

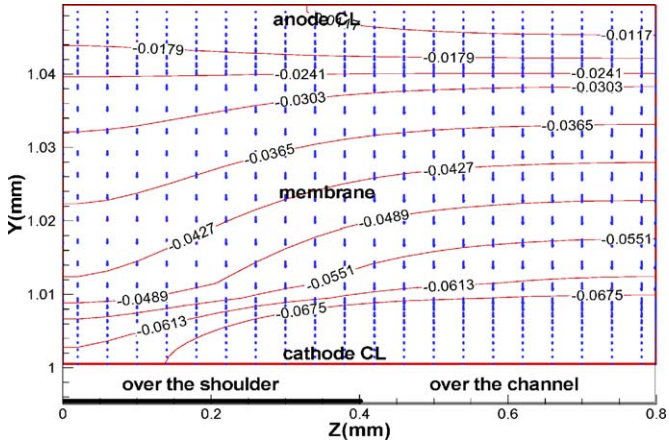

Fig. 4. Membrane-phase potential and proton transportation within MEA, $x = 0.2$ m. Current density = 0.7817 A cm^{-2}, cell voltage = 0.7 V.

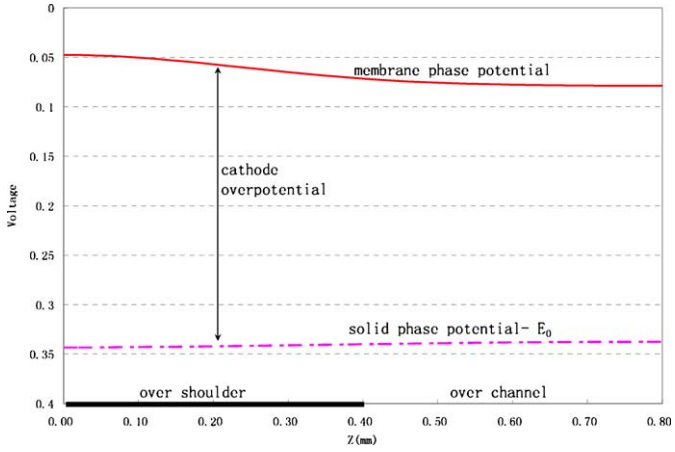

Fig. 5. Profiles of phase potentials across the z-direction, $x = 0.2$ m, $y = 1.04$ mm.

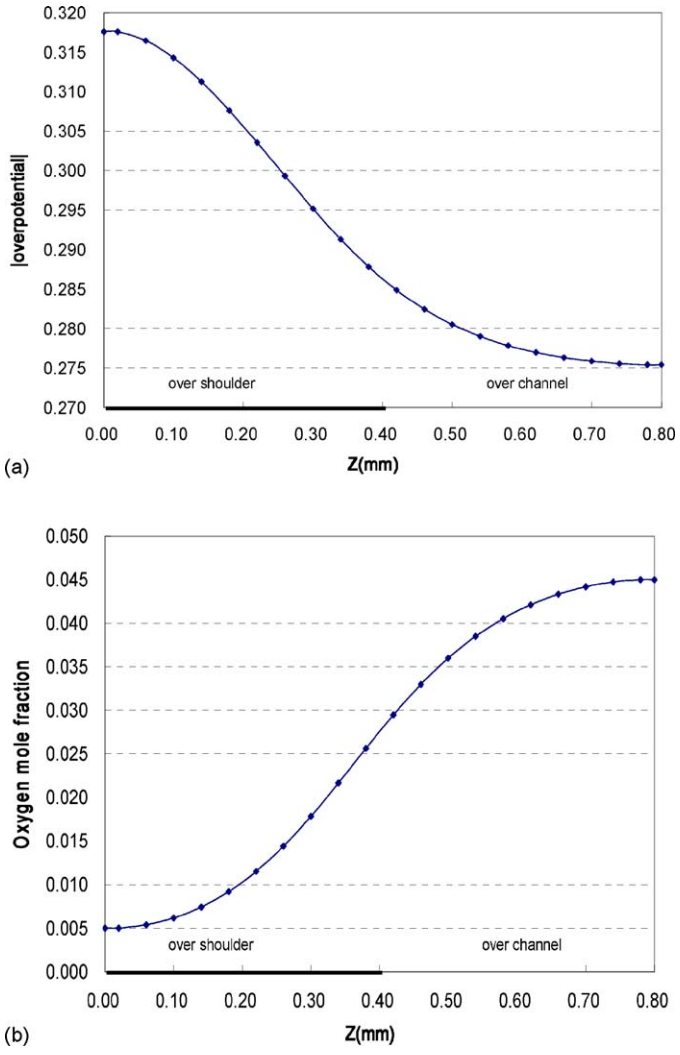

Fig. 6. Profiles of (a) the absolute values of overpotential (b) oxygen mole concentration across the z-direction, $x = 0.2$ m, $y = 1.04$ mm.

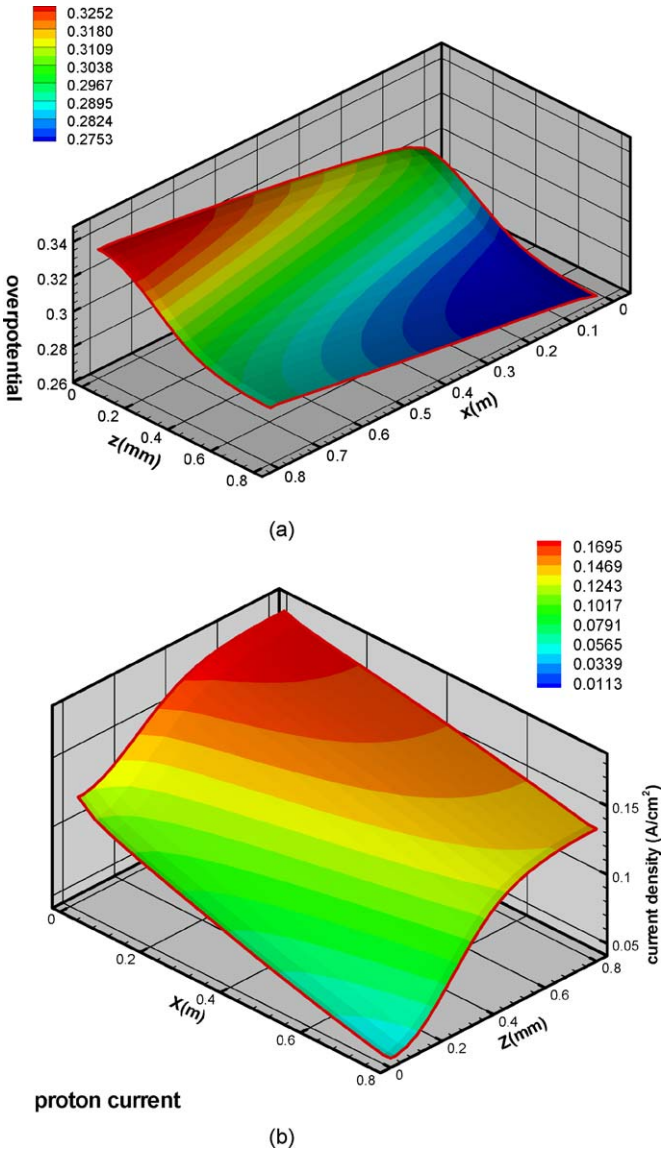

Fig. 7. (a) Overpotential values (absolute values) inside catalyst layer across oxz plane (b) proton current density across oxz plane, $y = 1.04$ mm.

($0 < z < 0.4$), the value of overpotential is higher, but the current density is lower (Fig. 7b). Because the magnitude of the reaction is the results of the two opposing factors: oxygen concentration and overpotential. In the base case, the variation of overpotential is not large enough to counter the effect of oxygen concentrations variations. Thus the current density is still higher where oxygen concentration is higher, though the overpotential value is slightly lower there.

Fig. 8 shows the change of phase potentials along the y-direction within the fuel cell. Due to the order of magnitude difference in length scales, the y-dimension is enlarged by non-dimentionlizing the y distance in each layer by the individual layer's thickness. The cathode overpotential is significantly larger than the overpotential at the anode. Another large voltage loss is the ohmic loss within the MEA due to proton current. The ohmic losses due to electron current (the solid-phase potential drops) at both the anode and cathode are very small.

Fig. 9 shows the polarization curves for Cases 1–5. The power reduction at current density of 0.8 A/cm^2, when compared with Case 5 (no electrical resistance) and Case 2 are listed in Table 2.

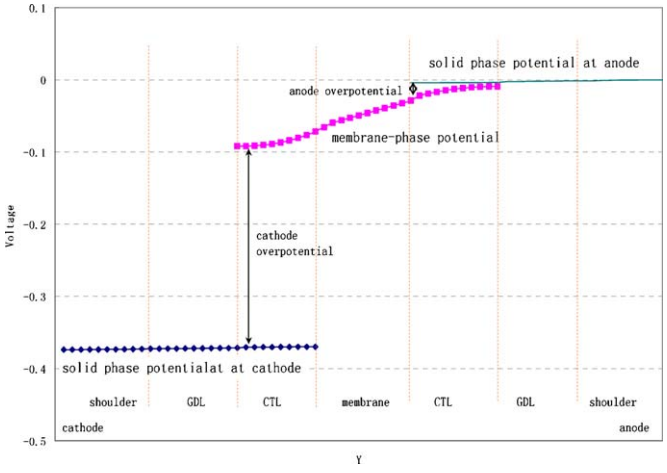

Fig. 8. The voltage losses within fuel cell.

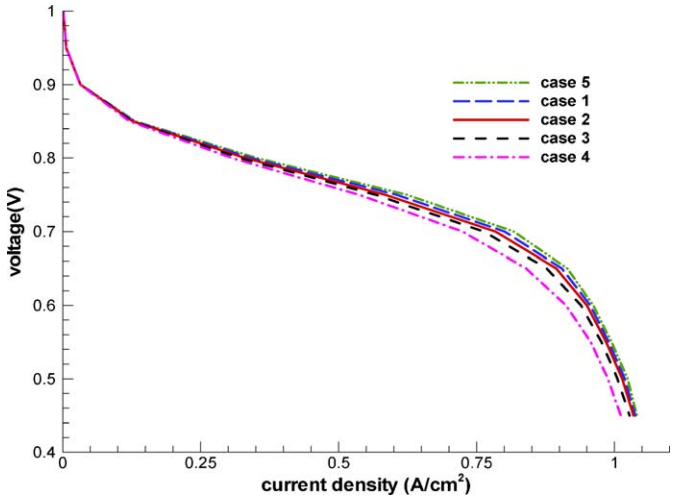

Fig. 9. Comparison of polarization curves for Cases 1–5. Case 1, $\sigma_{e,x}^{GDL} = \sigma_{e,z}^{GDL} = 17200\,S/m$, $\sigma_{e,y}^{GDL} = 1250\,S/m$; Case 2, $\sigma_{e,x}^{GDL} = \sigma_{e,z}^{GDL} = 1500\,S/m$, $\sigma_{e,y}^{GDL} = 300\,S/m$; Case 3, $\sigma_{e,x}^{GDL} = \sigma_{e,z}^{GDL} = \sigma_{e,y}^{GDL} = 300\,S/m$; Case 4, $\sigma_{e,x}^{GDL} = \sigma_{e,z}^{GDL} = 100\,S/m$, $\sigma_{e,y}^{GDL} = 300\,S/m$; Case 5, not considering electrical losses.

The power reduction in the base case is less than 1%. In Case 2, the electrical conductivities in the in-plane and through-plane directions are reduced to 300 and 1500 S m^{-1}, respectively, and the power reduction is still less than 2%. In case 3, the electrical conductivities in all three directions are reduced to 300 S m^{-1}, as was used in [1]. This caused a corresponding power reduction of about 3%. In Case 4, the electrical conductivity in the in-plane direction is disproportionably reduced to 100 S m^{-1}. The power reduction amounts to about 5%. Cases 2–4 have same electrical conductivity in the though-plane directions. Traditionally, the electrical resistance of GDL is estimated with this equation:

$$R = \int_{GDL} \frac{dy}{\sigma_{e,y}} \approx \frac{L}{\sigma_{e,y}} \tag{20}$$

From this equation, the cell voltage output should be the same for these three cases since only the electronic conductivity in the through-plane direction is directly used. However, for Cases 3 and 4 the power reductions are about 1.3% and 3.7% when

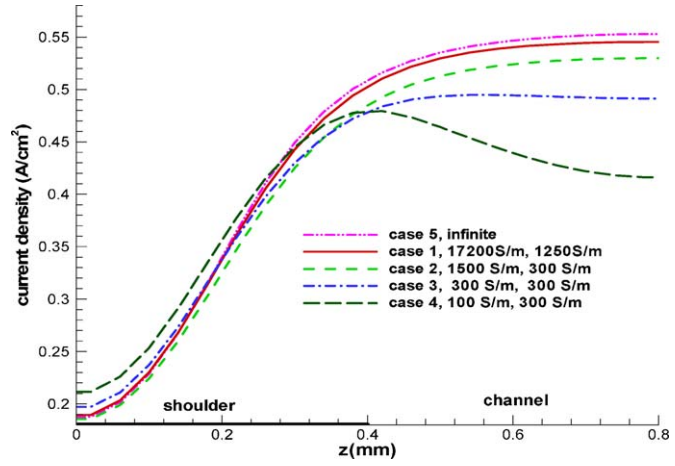

Fig. 10. Profiles of proton currents inside catalyst layer, cell voltage = 0.8 V.

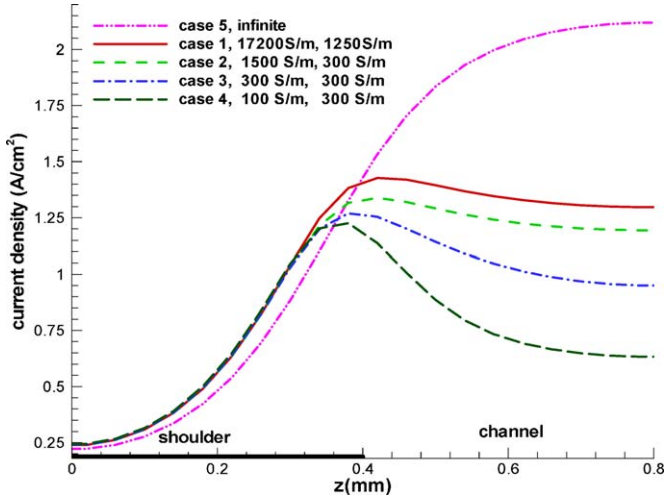

Fig. 11. Profiles proton current density inside catalyst layer, cell voltage = 0.5 V.

compared with Case 2. These differences are the effects of the electrical resistance in the in-plane direction. The change of electrical conductivity in the in-plane directions leads to changes in overpotential distribution and current distribution that reduces the predicted power output.

Figs. 10 and 11 show the distribution of proton current inside the catalyst layer for two different cell voltages. At a higher cell voltage (lower current density) as shown in Fig. 10, the highest current densities are over the channel in Cases 5, 1 and 2. But when the electrical resistance is much greater (not realistic) such as in Cases 3 and 4, the highest current density occurs at the boundary between the channel and the collector plate shoulder. This phenomenon is shown more clearly in Fig. 11 when the current density is higher (or lower cell voltage). In Fig. 11, all cases except case 5, in which the electrical resistance is not considered, have the largest current density near the edge between the shoulder and channel. This phenomenon is obviously the result of the combined effects of oxygen concentration and overpotential. Fig. 12 shows the changes of proton current density profiles

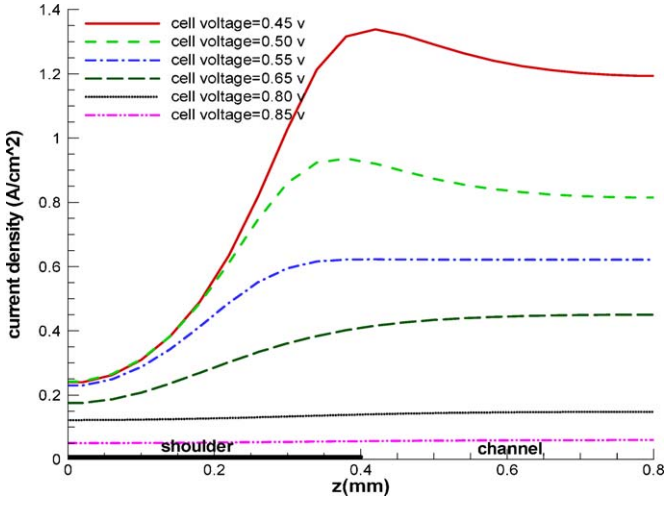

Fig. 12. Profiles proton current density inside catalyst layer for Case 2 under different cell voltages.

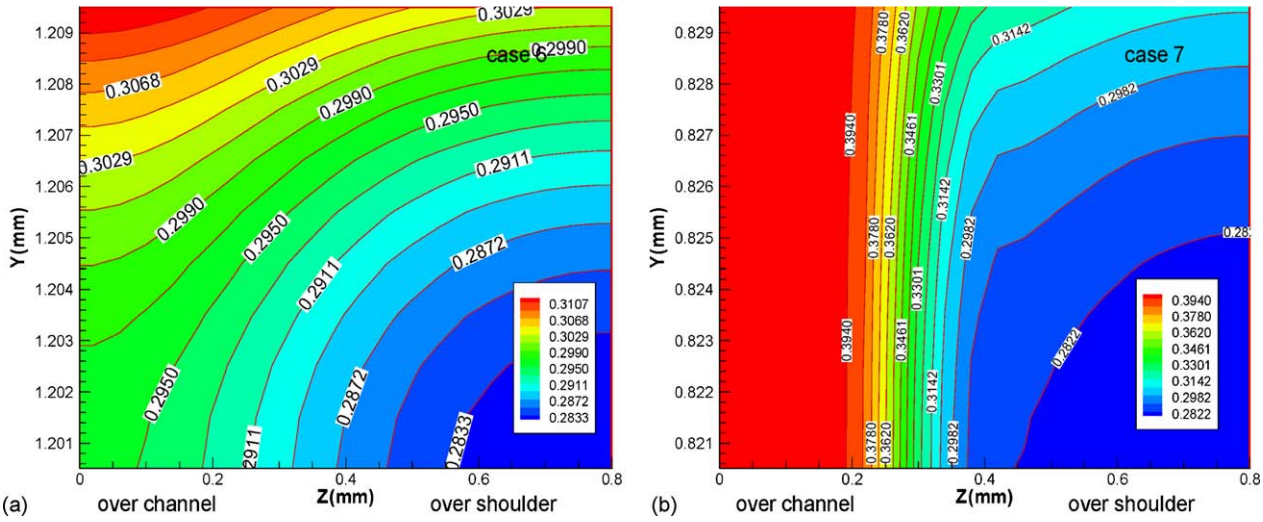

Fig. 13. The overpotential distribution within the cathode catalyst layer for (a) Case 6 and (b) Case 7. Cell voltage = 0.7 V, both cases have average overpotential about 0.29 V.

inside catalyst layer for Case 2 at different cell voltages (or current densities). Similar to what shown in Figs. 10 and 11, at higher current density (lower cell voltage), the maxim current density can occur over the boundary between the channel and the shoulder. But overall, the current density is sill larger over the channel where there is more oxygen.

Comparing Cases 1–5, it can be concluded that the influence of GDL electrical resistance depends on the values of the electrical conductivity (both in-plane and through-plane). The electrical conductivity in the through-plane direction affects the ohmic losses directly such as described by Eq. (20). The electrical conductivity in the in-plane direction influences the distribution of overpoetntial and local current density. If these influences are large enough, they could affect the power output. For the base case, where reasonable values of GDL and catalyst layer electrical conductivities are used, the influence of electrical conductance is negligible.

To further investigate the potential dominant effect of the GDL electrical resistance, cases with the GDL thickness doubled (Case 6) and reduced ten times (Case 7) were also studied. Fig. 13 shows the overpotential distribution within the cathode catalyst layer for Cases 6 and 7. When the GDL thickness is doubled (Fig. 13(a)), the variations in both the overpotential and the oxygen concentration reduce significantly due to the lower resistances to electron and mass transfers. Thus the current density distributions are relatively uniform in the z-direction as shown in Fig. 14 (a). When the GDL thickness is reduced as much as 10 times in Case 7, the variations of operpotential become more pronounced due to the increased resistance to the electronic conduction in the GDL as shown in Fig. 13 (b). Even under such an exaggerated case, the characteristics of the current density distribution remain the same, i.e. higher current over the channel and lower over the shoulder as shown in Fig. 14(b). This is obviously caused by the even more drastic reduction in the oxygen concentration over the shoulder when the GDL is extremely thin.

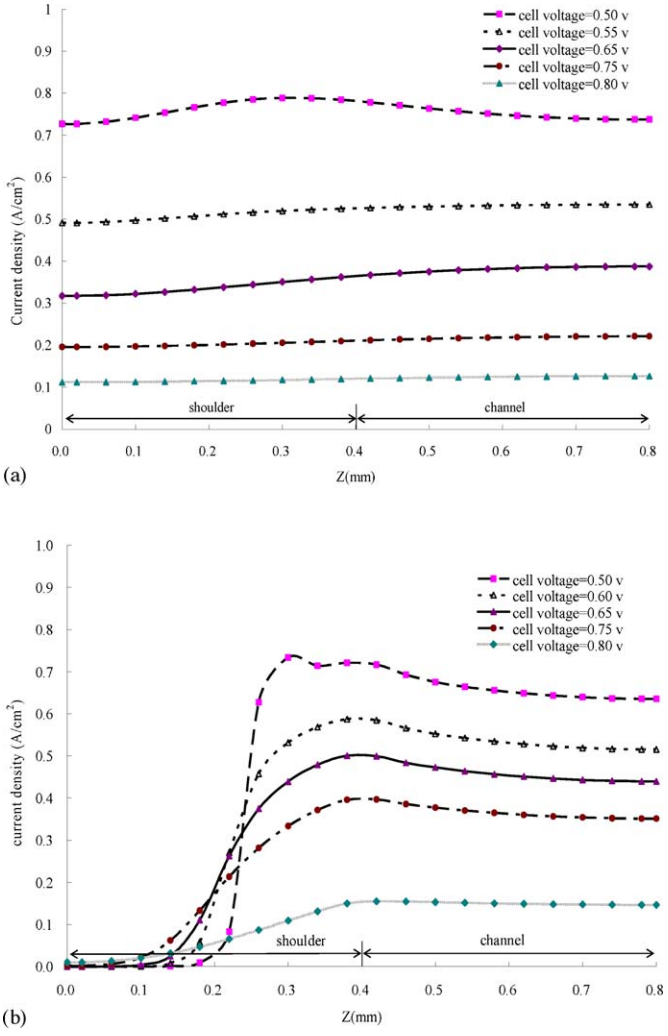

Fig. 14. Profiles proton current density inside catalyst layer for (a) Cases 6 and (b) Case 7.

4. Conclusions

A 3D fuel cell model incorporating the transport of electrons in the GDL and the catalyst layers is developed and employed to study the effects of the electrical resistance on current density distribution and cell power output. The highly anisotropic nature of the electrical conductivities of the commonly used GDL materials is taken into considerations. Using realistic values GDL conductivities in both the in-plane and through-plane directions, it has been shown that the effect of GDL electronic resistance is negligible. Additionally, the results of several cases, where much higher electrical resistances are used, are also presented. The results show even the electrical resistance of the GDL is increased by an order of magnitude, the characteristics of the current density distribution remains the same: higher over the channel and lower over the shoulder. To further explore possible situations where the GDL electrical resistance could be significant, cases with both thicker and much thinner GDL have been studied. The results show again that the characteristics of the current density distributions remain the same. Therefore it can be concluded that unless a total different material is used as the GDL, or in some extreme cases, the electrical resistance of the GDL can be neglected in the design and optimization of PEM fuel cells.

References

[1] H. Meng, C.Y. Wang, Electron transport in PEFCs, J. Electrochem. Soc. 151 (2004) A358–A367.
[2] B.R. Sivertsen, N. Djilali, CFD-based modeling of proton exchange membrane fuel cells, J. Power Sources 141 (2005) 65–78.
[3] T. Zhou, H.T. Liu, A general three-dimensional model for proton exchange membrane fuel cells, Int. J. Transport Phenom. 3 (2001) 177–198.
[4] H.T. Liu, T. Zhou, Fuel Cell Performance Augmentation by Mass Transfer Enhancement, J. Enhanced Heat Transfer 10 (2003) 257–274.
[5] W. Sun, B.A.P. Peppley, K. Karan, Influence of gas diffusion layer and channel geometry parameters on catalyst performance: investigation using a 2-D model, J. Power Sources 144 (2005) 42–53.
[6] M.V. Williams, E. Begg, L. Bonville, H.R. Kunz, J.M. Fenton, Characterization of gas diffusion layers for PEMFC, J. Electrochem. Soc. 151 (2004) A1173–A1180.
[7] F. Barbir, PEM Fuel Cells: Theory and Practice, Academic Press, 2005, June 21.
[8] V. Gurau, H.T. Liu, S. Kakac, Two-dimensional model for proton exchange membrane fuel cells, AIChE J. 44 (1998) 2410–2422.
[9] D.M. Bernardi, M.W. Verbrugge, A mathematical model for the solid-polymer-electrode fuel cell, J. Electrochem. Soc. 139 (1992) 2477–2490.
[10] T.E. Springer, T.A. Zawodzinski, S. Gottesfeld, Polymer electrolyte fuel cell model, J. Electrochem. Soc. 138 (1991) 2334–2342.
[11] P.D. Beattie, V.I. Basura, S. Holdcroft, Temperature and pressure dependence of O_2 reduction at Pt|Nafion® 117 and Pt|BAM® 407 interfaces, J. Electroanal. Chem. 468 (1999) 180–192.
[12] D. Dagan, Flow and Transport in Porous Formations, Springer-Verlag, 1989.
[13] D. Pantea, H. Darmstadt, S. Kaliaguine, C. Roy, Electrical conductivity of conductive carbon blacks: influence of surface chemistry and topology, Appl. Surf. Sci. 217 (2003) 181–193.